RESEARCH ARTICLE | FEBRUARY 24 2026

Exchange bias effect in thin Fe_3GeTe_2 and Fe_5GeTe_2 flakes sensitive to oxidation and annealing methods FREE

A. M. Abdallah ; H. Arisawa ; Y. Nonaka ; Y. Kasai; R. Fujikawa; E. Saitoh ; J. Haruyama

Appl. Phys. Lett. 128, 082403 (2026)
https://doi.org/10.1063/5.0312737

Applied Physics Letters ARTICLE pubs.aip.org/aip/apl

Exchange bias effect in thin Fe_3GeTe_2 and Fe_5GeTe_2 flakes sensitive to oxidation and annealing methods

Cite as: Appl. Phys. Lett. **128**, 082403 (2026); doi: 10.1063/5.0312737
Submitted: 18 November 2025 · Accepted: 5 February 2026 ·
Published Online: 24 February 2026

A. M. Abdallah,[1] H. Arisawa,[2] Y. Nonaka,[1] Y. Kasai,[1] R. Fujikawa,[1] E. Saitoh,[2,3,4,5] and J. Haruyama[1,6,a)]

AFFILIATIONS

[1]Faculty of Science and Engineering, Aoyama Gakuin University, 5-10-1 Fuchinobe, Sagamihara, Kanagawa 252-5258, Japan
[2]Department of Applied Physics, The University of Tokyo, 7-3-1 Hongo, Bunkyo-ku, Tokyo 113-8656, Japan
[3]Institute for AI and Beyond, The University of Tokyo, 7-3-1 Hongo, Bunkyo-ku, Tokyo 113-8656, Japan
[4]WPI Advanced Institute for Materials Research, Tohoku University, 2-1-1 Katahira, Aoba-ku, Sendai 980-8577, Japan
[5]Advanced Science Research Center, Japan Atomic Energy Agency, 2-4 Shirakata, Tokai-mura, Naka-gun, Ibaraki 319-1195, Japan
[6]Institute of Industrial Sciences, The University of Tokyo, 4-6-1 Komaba Meguro-ku, Tokyo 153-8505, Japan

[a)]**Author to whom correspondence should be addressed:** junjiharuyama@yahoo.co.jp

ABSTRACT

The exchange bias (EB) effect—an asymmetric shift in the ferromagnetic (FM) hysteresis loop arising from the coupling between bulk FM and surface antiferromagnetic (AFM) spin alignments in FM materials—has attracted considerable attention. Owing to their weak interlayer FM spin-coupling and facile surface oxidation that promotes AFM spin formation, thin van der Waals (vdW) magnetic materials provide an ideal platform for investigating the EB effect. In this study, we fabricate thin vdW magnetic flakes of Fe_3GeTe_2 (F_3GT) and Fe_5GeTe_2 (F_5GT) and subject them to both natural and intentional oxidation under ambient air. It is found that intentionally oxidized F_3GT flakes exhibit an enhanced EB effect, approximately 2.5 times larger than that of naturally oxidized flakes, owing to homogeneous surface oxidation. In contrast, F_5GT flakes display an AFM spin phase with the negligible EB effect in both naturally and intentionally oxidized samples. However, high-temperature annealing of the intentionally oxidized F_5GT flakes under vacuum eliminates the AFM phase, leading to the emergence of diamagnetism superimposed with a pronounced EB-like effect, which is approximately 1.5–2.5 times greater than that observed in intentionally oxidized F_3GT. These findings demonstrate innovative strategies for controlling and inducing the EB effect, paving the way for its potential spintronic applications.

Two-dimensional (2D) van der Waals (vdW) (anti)ferromagnets have exhibited unique spintronic and magnetic properties, making them promising candidates for next-generation spintronic devices. Representative examples include CrI_3,[1,2] CrSBr,[3] Fe_3GeTe_2 (F_3GT),[4–12] Fe_5GeTe_2 (F_5GT),[13–18] and Fe_3GaTe_2.[19] Among these materials, F_3GT and F_5GT stand out due to their distinctive physical characteristics, such as high Curie temperatures (T_C), large anomalous Hall effects, pronounced exchange bias (EB) effects, high tunnel magnetoresistance (TMR) ratios, and stable magnetic skyrmions.

Among these phenomena, the exchange bias (EB) effect is particularly intriguing.[8–11,16–18] It is characterized by the appearance of an asymmetric magnetic hysteresis loop, that is, unequal coercivities under positive and negative magnetic fields (H). This effect is caused by cooling the sample from room T under a constant applied $+H$ or $-H$. The EB effect conventionally originates from the formation of interfacial spin coupling between bulk ferromagnetic (FM) regions and surface antiferromagnetic (AFM) layers during the cooling process. While the AFM phase is relatively insensitive to the applied H direction, the FM spin moments align with the constant $\pm H$ during cooling and become strongly coupled with the surface AFM spins at the interface, resulting in an interfacial spin-coupling moment opposite to the applied H. This interfacial coupling is robust; consequently, the FM spins at the topmost layer in the bulk region resist reversal under alternating $\pm H$ during subsequent magnetization (M)–H curve measurements at low T, giving rise to the EB effect.

This effect becomes particularly pronounced in thin two-dimensional (2D) magnetic materials such as F_3GT, where the weak interlayer FM spin coupling in the bulk enhances the relative contribution of surface interactions. Surface oxidation in such systems facilitates the formation of AFM spin alignment at the interface, thereby

strengthening the EB effect.[5,20,21] This can be significant in Fe-based 2D magnetic layers, as Fe–O coupling leads to a strongly reinforced AFM interaction.

The EB effect has been reported in various 2D magnetic layers, e.g., 2D-intrinsic F_3GTs,[8–10] F_3GT-based artificial AFM/FM layers,[11] 2D-intrinsic F_5GTs,[16] and F_5GT-based artificial layers.[17,18] Although the artificial AFM/FM materials have yielded large EB effect (e.g., ∼1400 Oe in F_5GT/V_2O_5 or Al_2O_3), the correlation of the EB effect with oxidation, defects, and annealing conditions in intrinsic F_3GT and F_5GT has not been almost reported.

Here, we reveal that intentionally oxidized thin intrinsic F_3GT flakes exhibit an EB effect, ∼1.5 times greater than that of naturally oxidized flakes. In contrast, thin intrinsic F_5GT flakes display an AFM spin phase with almost no observable EB effect in both naturally and intentionally oxidized samples. However, high-T annealing of the intentionally oxidized F_5GT flakes under low vacuum leads to the emergence of diamagnetism superimposed with a pronounced EB-like effect, which is ∼1.5–2.5 times stronger than that observed in the intentionally oxidized F_3GT.

Thin flakes of F_3GT and F_5GT [Figs. 1(a) and 1(b)] are fabricated by mechanically exfoliating bulk crystals onto Si/SiO_2 substrates. Each substrate contains approximately five flakes, with areas ranging from ∼20 to 100 μm2 for F_3GT and ∼10 to 50 μm2 for F_5GT. We measure the average magnetic response of these flakes on each substrate because the fabrication of large-area thin $F_{3(5)}GT$ flakes is very difficult, and the magnetization of individual flakes is too small to be accurately detected owing to noise.

Representative atomic force microscopy images of the flakes are shown in Figs. 1(c)–1(f), including top views [Figs. 1(c) and 1(d)] and cross-sectional profiles with thicknesses of ∼38 and ∼22 nm for F_3GT

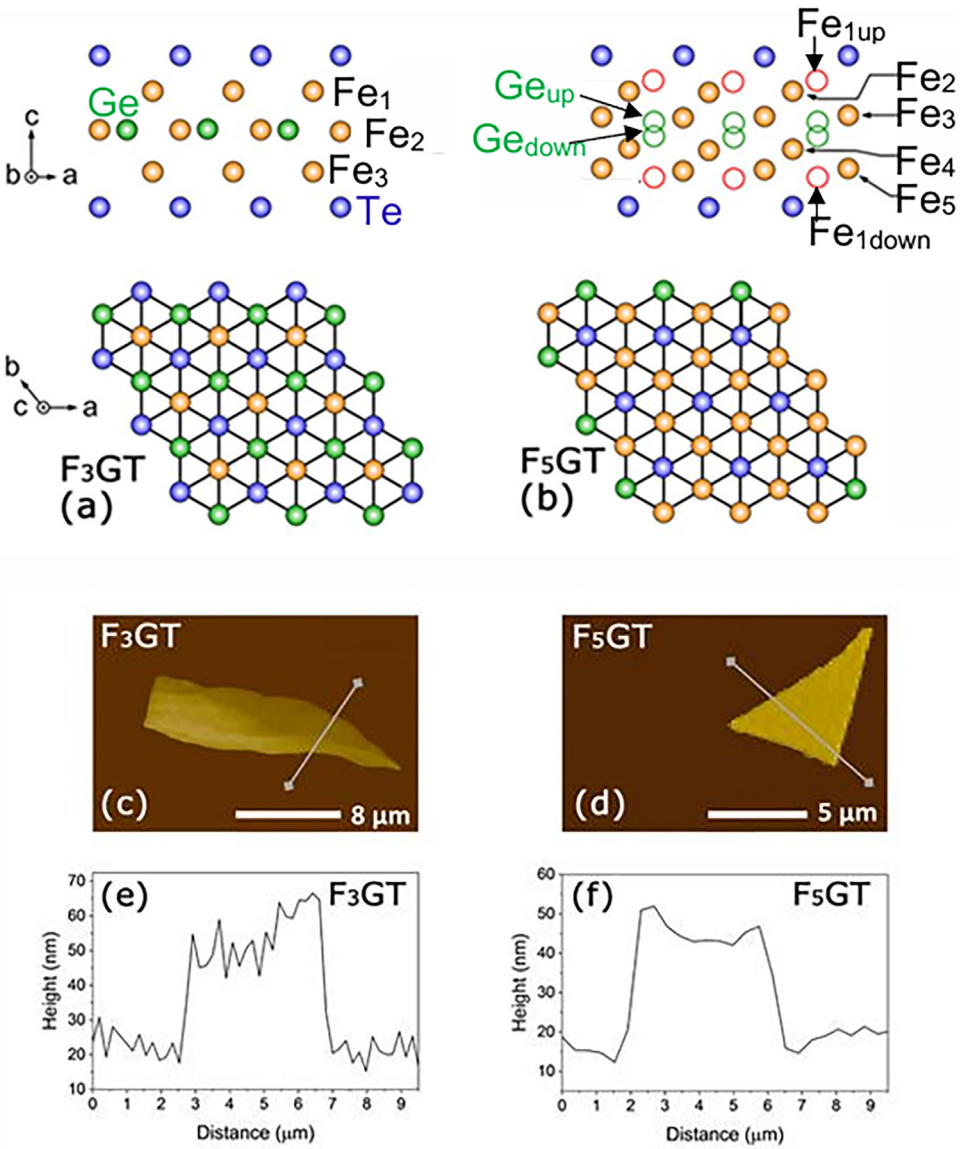

FIG. 1. Schematic views of (a) F_3GT and (b) F_5GT crystal lattices. Upper and lower panels correspond to cross-sectional and top views, respectively. AFM images of (c) and (e) F_3GT and (d) and (f) F_5GT flakes. (c) and (d) and (e) and (f) correspond to top and cross-sectional views, respectively.

and F_5GT, respectively [Figs. 1(e) and 1(f)]. The flakes are subjected to either natural or intentional oxidation. For natural oxidation, samples are exposed to ambient air at room T for 3 days. For intentional oxidation, samples are annealed at ∼100 °C for 30 min in ambient air.

The M values of the flakes are measured under out-of-plane H using a superconducting quantum interference device (SQUID; Quantum Design, MPMS3). To observe the EB effect, the samples are cooled from room temperature to 2 K under a constant out-of-plane H of either +2500 or −2500 Oe. The strength of the EB effect $H_{EB} = (H_{c+} + H_{c-})/2$, where H_{c+} and H_{c-} denote the positive and negative coercive Hs, respectively, is obtained from the M–H hysteresis curves.

Figures 2(a) and 2(b) show the M–H curves of naturally and intentionally oxidized F_3GT flakes, respectively, measured at $T = 2$ K after positive and negative H cooling. Evident asymmetry is observed in the M–H loops for both samples. The samples cooled under $+H$ exhibit larger H_{c-} values along with higher positive saturation magnetization (M_s), whereas those cooled under $-H$ show larger H_{c+} values and higher negative M_s. Notably, the H_{EB} value (∼175 Oe) of the intentionally oxidized F_3GT is ∼2.5 times greater than that (∼75 Oe) of the naturally oxidized sample after $+H$ cooling.

The M–H hysteresis loops also exhibit a vertical shift along the M axis. One possible cause for this shift—an asymmetric displacement of the residual magnetization (M_r)—is the markedly different densities of residual spins accumulated at $H = 0$, arising from the different H_{c+} and H_{c-} values induced by the EB effect. For instance, H_{c-} increases after the fixed H of +2500 Oe cooling. This behavior suggests that a large spin moment aligned with the applied constant $+H$ direction couples to the surface AFM spins in the top region of the F_3GT layers and accumulates there because a larger H_{c-} is required to compensate for this accumulated spin moment. This accumulation manifests itself as a large positive M_r.

The T dependence of H_{EB} for all F_3GT samples, including the results shown in Figs. 2(a) and 2(b) at $T = 2$ K, is presented in Fig. 2(c). The intentionally oxidized samples exhibit H_{EB} values that are consistently higher than those of the naturally oxidized samples across all T, except for the case of $-H$ cooling at 2 K described earlier, although H_{EB} rapidly decreases with increasing T and nearly vanishes around $T \approx 30$ K.

On the other hand, results of similar M–H measurements for F_5GT samples, subjected to the same oxidation procedures as those applied to F_3GT, are presented in Fig. 3. In contrast to F_3GT (Fig. 2), the FM hysteresis is almost completely suppressed, while AFM M–H behavior is observed in all samples with a slightly asymmetric hysteresis loop only in Fig. 3(a) (see inset).

Figure 4(a) shows the M–H curves of the sample from Fig. 3(b) after high-T annealing under vacuum (500 °C, 0.02 Pa, 5 min). The AFM M–H behavior observed in Fig. 3 is completely suppressed, while diamagnetic M–H curves with superimposed FM-like hysteresis and a pronounced EB-like effect ($H_{EB} \sim 250$ Oe) are observed, ∼1.5 times larger than those in Fig. 2(b). Remarkably, this EB-like effect persists up to higher T [≫50 K; Fig. 4(b)], in contrast to the T-dependent EB behavior observed in Fig. 2(c), implying ∼1.5–2.5 times larger values depending on T.

The difference in the extent of oxidation between F_3GT and F_5GT strongly depends on the number of Fe sites, i.e., three in F_3GT

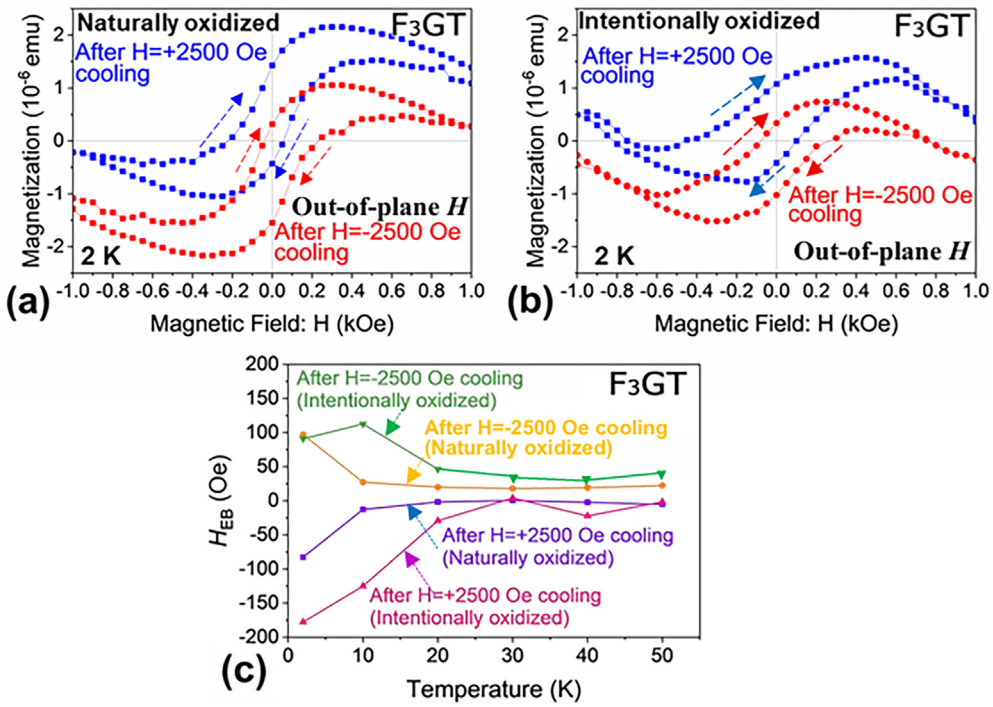

FIG. 2. M–H curves of (a) the naturally and (b) the intentionally oxidized F_3GT flakes measured with out-of-plane H after the sample cooling with applying constant out-of-pane $H = +2500$ or -2500 Oe. (c) Temperature dependence of the EB effect values (H_{EB}) of the naturally and intentionally oxidized F_3GT flakes including the results of (a) and (b).

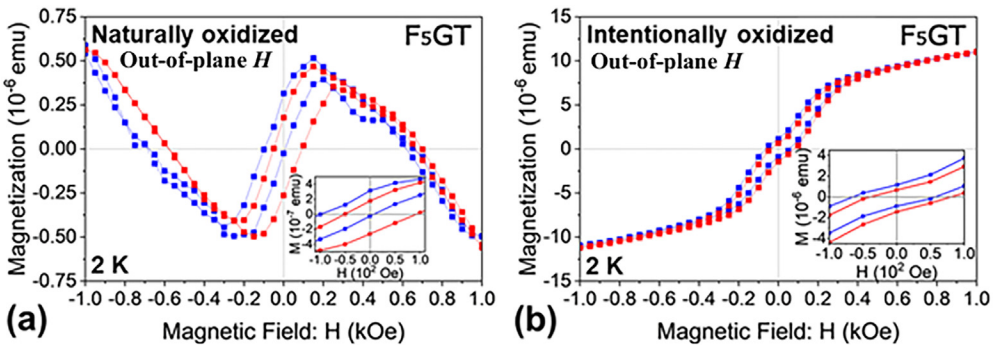

FIG. 3. *M–H* curves of (a) the naturally and (b) the intentionally oxidized F_5GT flakes measured with out-of-plane *H* after the sample cooling with applying constant with out-of-plane $H = +2500$ or -2500 Oe. Insets: zoom of main panels.

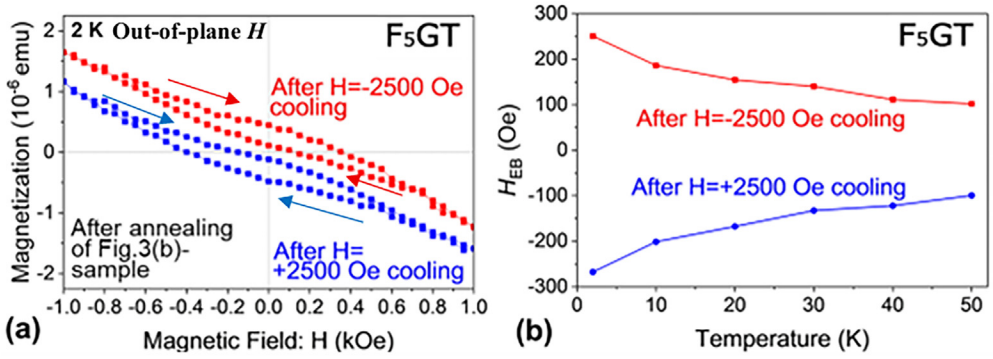

FIG. 4. (a) *M–H* curves of Fig. 3(b)-sample after the high-*T* annealing at 500 °C under vacuum, measured with out-of-plane *H* after the sample cooling with applying constant with out-of-plane $H = +2500$ or -2500 Oe. (b) Temperature dependence of H_{EB} including the results of (a).

and five in F_5GT. In particular, in F_5GT, only the top and bottom Fe-atomic layers within a single quantum layer host spin-up and spin-down sites [Fig. 1(b)]. Oxidation of these surface Fe sites results in a greater degree of oxidation, as they are more susceptible to oxidation. On the other hand, the reduced magnetization observed after oxidation in F_5GT [Fig. 3(a)] is attributed to the suppression of FM due to the emergence of AFM ordering induced by oxidation. As mentioned earlier, the larger extent of oxidation in F_5GT facilitates the formation of this AFM phase.

Here, we discuss a qualitative interpretation of the three main observations: (1) the H_{EB} values of intentionally oxidized F_3GT flakes, ~2.5 times greater than that in the naturally oxidized sample (Fig. 2); (2) the appearance of AFM *M–H* curves with slight FM asymmetry in F_5GT flakes (Fig. 3); and (3) the emergence of diamagnetic *M–H* curves with the superimposed EB-like effect, which is ~1.5–2.5 times larger than those in the intentionally oxidized F_3GT flakes, in the high-*T*, vacuum-annealed sample from Fig. 3(b) (Fig. 4).

For (1), intentionally oxidized F_3GT flakes exhibited H_{EB} values ~2.5 times greater than those of the naturally oxidized sample (Fig. 2). Figures 5(a) and 5(b) show cross-sectional high-resolution transmission electron microscopy (HRTEM) images of the surface regions of these two samples. In both cases, the topmost layers are clearly oxidized. The interface between the surface-oxidized and bulk non-oxidized regions is relatively uniform in the intentionally oxidized sample [Fig. 5(b)] compared with the naturally oxidized sample [Fig. 5(a)]. In the naturally oxidized sample, where the flakes were simply exposed to ambient air at room *T* for an extended period, oxidation occurs randomly across the surface [Fig. 5(a)]. By contrast, in the intentionally oxidized sample, uniform heating from the substrate side results in homogeneous surface oxidation [Fig. 5(b)].

As explained above, the EB effect arises from interfacial spin coupling between bulk FM regions and surface AFM layers, and it becomes more pronounced in thin 2D magnetic materials such as the present F_3GT flakes, where interlayer FM spin coupling in the bulk is weak, enhancing the relative contribution of interfacial coupling with surface AFM layers. Consequently, the uniform surface-oxidized layers in intentionally oxidized samples enlarge the area of strong interfacial coupling between surface AFM and bulk FM spins [Fig. 5(c)], resulting in the observed enhancement of the EB effect.

For (2), AFM behavior with slight FM *M–H* asymmetry, like an EB effect, was observed in F_5GT flakes, in contrast to F_3GT (Fig. 3). This behavior can be attributed to the oxidation of the numerous Fe-atom vacancies inherent to the complex lattice structure of F_5GT, which contains multiple Fe sites [Fig. 1(b) and right panel of Fig. 5(d)]. It is well established that oxidation at Fe-atom vacancy-sites in F_5GT stabilizes AFM spin states. Furthermore, since the thin F_5GT flakes were mechanically exfoliated using Scotch tape, additional Fe-atom vacancies are likely introduced, particularly at the surface [left panel if

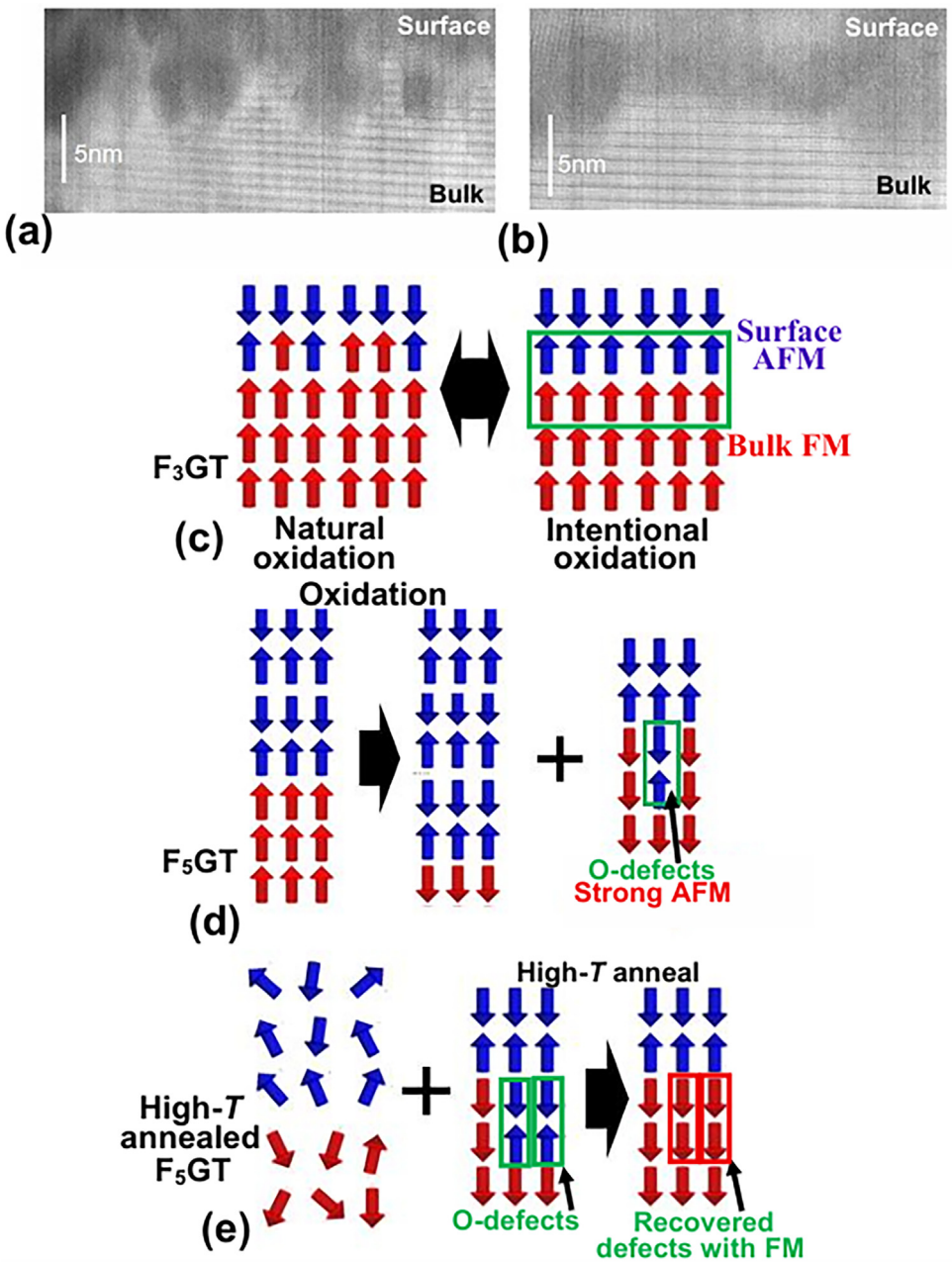

FIG. 5. (a) and (b) Cross-sectional HRTEM images of the surface regions of (a) the naturally and (b) the intentionally oxidized F_3GT flakes. Darker parts without lattice structure at the surface side correspond to oxidized regions. (c) and (e) Schematic views of spin models to interpret the observed three main results. (c) The large EB effect in the intentionally oxidized F_3GT, (d) he AFM behavior in the oxidized F_5GT, and (e) the diamagnetism with the strong EB-like effect in the high-T and vacuum-annealed (d)-sample.

Fig. 5(d)]. Although this has not yet been experimentally confirmed, the crystal structure of F_5GT with five Fe sites is highly complex and is known to be that attaching Scotch tape to the sample surface tends to introduce Fe-vacancy defects at these sites, particularly at the topmost surface of flakes.[14–17] Consequently, AFM behavior dominates the M–H response, while the small remaining FM regions give rise to the observed EB-like hysteresis with slight asymmetry.

For (3), high-T annealing of the sample from Fig. 3(b) under low vacuum transformed the AFM M–H curves into diamagnetic curves with superimposed ferromagnetic-like hysteresis, giving rise to a pronounced EB-like effect approximately 1.5–2.5 times larger than that observed in F_3GT, depending on T (Fig. 4). The emergence of diamagnetism can be attributed to partial lattice destruction to yield FM (or AFM) spin alignments, caused by the excessively high annealing T, which was not optimized to preserve the crystal structure [left panel of Fig. 5(e)]. Two possible mechanisms may account for the observed diamagnetism: (a) the emergence of intrinsic diamagnetism in the Fe_5GT flakes themselves resulting from partial lattice destruction and activation of some O-coupled atomic sites induced by high-T annealing with oxidation, and (b) the suppression of FM in the flakes due to lattice

destruction and appearance of diamagnetism in Si substrate caused by high-T annealing with oxidation.

For (a), O–Fe coupling is known to favor FM, and, thus, coupling involving Ge–O or Te–O bonds may instead be responsible for the emergence of diamagnetism. For (b), the Si substrates used in this study contain a small amount of Nb. If a fraction of Nb atoms is present near the substrate surface, O–Nb coupling may induce diamagnetic behavior. Indeed, diamagnetism was observed in some substrates without flakes subjected to the same low-pressure annealing conditions. The diamagnetic response becomes significant, as in the present case, only when the diamagnetism originating from the substrate is much larger than the reduced FM contribution from the F_5GT flakes.

On the other hand, the appearance of the EB-like effect can be ascribed to partial recovery of oxidized Fe-atom vacancy-sites in regions where the crystal structure remained intact during high-T vacuum annealing [right panel of Fig. 5(e)]. Although this leads to only partial restoration of FM spin regions, the observed EB-like effect is substantially larger than that in intentionally oxidized F_3GT up to the high-T regions. These observations suggest that defect-free oxidized F_5GT could potentially exhibit an even stronger EB effect, as F_5GT contains numerous Fe sites, including spin-split sites [Fe_{1up} and Fe_{1down} in Fig. 1(b)]. Coupling of these spin-split sites in the topmost bulk FM layers with surface AFM spins [Fig. 5(e)] could generate an enhanced EB effect up to the high-T regions. The observed results with the robust EB effect are qualitatively consistent with the large EB effect in the F_5GT-based artificial AFM/FM layers and the presence of the high T_c (>300 K) in F_5GT. Optimized high-T annealing is, therefore, expected to further confirm this hypothesis and achieve a greater EB effect even in intrinsic F_5GT flakes like the case of artificial AFM/F_5GT layers.

In conclusion, we have demonstrated that intentionally oxidized thin intrinsic F_3GT flakes exhibit an EB effect (H_{EB} value ~175 Oe), ~2.5 times greater than that of naturally oxidized flakes. In contrast, thin intrinsic F_5GT flakes displayed an AFM spin phase with negligible EB effect in both naturally and intentionally oxidized samples. However, high-T annealing of the intentionally oxidized F_5GT flakes under low vacuum transformed the M–H response into diamagnetic behavior with the superimposed EB-like effect, ~1.5–2.5 times larger than that observed in intentionally oxidized F_3GT depending on T. Although the observed H_{EB} values are much smaller than those in artificial AFM/FGT layers, the enhanced EB effect revealed in the present intrinsic FGT layers is valuable for further understanding of mechanisms of the EB effect and advance of this field. They provide a pathway for controlling and enhancing the EB effect, with potential implications for spintronic applications.

We thank S. Maruyama, S. Chiashi, R. Toda, T. Fujii, T. Ando, Y. Wu, D. Li, E. Tsymbal, and P. Kim for their technical contributions, fruitful discussions, and encouragement. The work at the Aoyama Gakuin University was partly supported by the Aoyama Gakuin University Research Institute grant program for the creation of innovative research. Work at the University of Tokyo was partly supported by JST-CREST (JPMJCR20C1 and JPMJCR20T2), Grant-in-Aid for Scientific Research (JP19H05600 and JP24K01326) and Grant-in-Aid for Transformative Research Areas (JP22H05114) from JSPS KAKENHI, MEXT Initiative to Establish Next-generation Novel Integrated Circuits Centers (X-NICS) (JPJ011438), Japan, and Institute for AI and Beyond of the University of Tokyo for E. S. K.W. and T.T. acknowledge support from the JSPS KAKENHI (Grant Nos. 20H00354, 21H05233, and 23H02052) and World Premier International Research Center Initiative (WPI), MEXT, Japan.

AUTHOR DECLARATIONS

Conflict of Interest

The authors have no conflicts to disclose.

Author Contributions

A. M. Abdallah: Conceptualization (equal); Data curation (lead); Investigation (lead); Writing – original draft (equal). **H. Arisawa:** Data curation (supporting). **Y. Nonaka:** Data curation (supporting). **Y. Kasai:** Data curation (supporting). **R. Fujikawa:** Data curation (supporting). **E. Saitoh:** Supervision (supporting). **J. Haruyama:** Conceptualization (lead); Supervision (lead); Writing – original draft (equal).

DATA AVAILABILITY

The data that support the findings of this study are available from the corresponding author upon reasonable request.

REFERENCES

[1]B. Huang, G. Clark, D. R. Klein *et al.*, Nat. Nanotechnol. **13**, 544 (2018).
[2]T. Song, X. Cai, M. W.-Y. Tu *et al.*, Science **360**, 1214 (2018).
[3]Y. Chen, K. Samanta, N. A. Shahed, H. Zhang, C. Fang, A. Ernst, E. Y. Tsymbal, and S. S. P. Parkin, Nature **632**, 1045 (2024).
[4]R. Obata, H. Sun, K. Samanta *et al.*, Adv. Mater. **37**, 2411459 (2025).
[5]R. Obata, M. Kosugi, Y. Oguchi, H. Sun, T. Kikkawa, C. Tomatsu, K. Suenaga, E. Saitoh, S. Maruyama, and J. Haruyama, Nanotechnology **35**, 475601 (2024).
[6]Z. Wang, D. Sapkota, T. Taniguchi, K. Watanabe, and A. F. Morpurgo, Nano Lett. **18**, 4303 (2018).
[7]H. Wang, H. Wu, J. Zhang *et al.*, Nat. Commun. **14**, 5173 (2023).
[8]H. K. Gweon, S. Y. Lee, H. Y. Kwon, J. Jeong, H. J. Chang, K.-W. Kim, Z. Q. Qiu, H. Ryu, C. Jang, and J. W. Choi, Nano Lett. **21**, 1672 (2021).
[9]S. Ma, G. Li, Z. Li, Y. Zhang, H. Lu, Z. Gao, J. Wu, G. Long, and Y. Huang, ACS Nano **16**, 19439 (2022).
[10]S. Hu, X. Cui, Z. Yue, P. Wang, L. Guo, K. Ohnishi, X. Wang, and T. Kimura, 2D Mater. **9**, 015037 (2022).
[11]Y. Zhang, H. Xu, C. Yi *et al.*, Appl. Phys. Lett. **118**, 262406 (2021).
[12]Y. Wu, S. Zhang, J. Zhang *et al.*, Nat. Commun. **11**, 3860 (2020).
[13]R. Fujita, P. Bassirian, Z. Li, Y. Guo, M. A. Mawass, F. Kronast, G. van der Laan, and T. Hesjedal, ACS Nano **16**, 10545 (2022).
[14]B. Zhao, R. Ngaloy, S. Ghosh *et al.*, Adv. Mater. **35**, 2209113 (2023).
[15]L. Alahmed, B. Nepal, J. Macy *et al.*, 2D Mater. **8**, 045030 (2021).
[16]C. Wang, K. Zhu, Y. Ma *et al.*, Phys. Rev. B **108**, 094408 (2023).
[17]S. Albarakati, W.-Q. Xie, C. Tan *et al.*, Nano Lett. **22**, 6166 (2022).
[18]J. Liang, S. Liang, T. Xie *et al.*, Phys. Rev. Mater. **7**, 014008 (2023).
[19]S. Wu, Z. He, M. Gu *et al.*, Nat. Commun. **15**, 10765 (2024).
[20]D. Kim, S. Park, J. Lee *et al.*, Nanotechnology **30**, 245701 (2019).
[21]Y. Li, X. Hu, A. Fereidouni *et al.*, ACS Appl. Nano Mater. **6**, 4390 (2023).